

Effects of Symmetry on Bulk-Edge Correspondence in Periodically Driven Systems

Derek Y.H. Ho¹ and Jiangbin Gong^{1,2,*}

¹*Department of Physics and Center for Computational Science and Engineering,*

National University of Singapore, 117542, Singapore

²*NUS Graduate School for Integrative Sciences*

and Engineering, Singapore 117597, Singapore

(Dated: March 31, 2014)

Abstract

Topological states of matter in periodically driven systems have been attracting great theoretical and experimental interests, but more insights need to be gained to better understand the issue of bulk-edge correspondence in driven systems. To that end, this work investigates in detail how specific properties of chiral symmetry operators may lead to a big difference in the behavior of the edge states. In particular, we exploit two dynamical models, namely, a variant of the so-called kicked-rotor model in the quantum chaos literature and the kicked Harper model, both possessing fractal-like quasi-energy spectra closely resembling the Hofstadter butterfly. Despite the topological equivalence between the two dynamical systems [H. Wang, D. Y. H. Ho, W. Lawton, J. Wang and J. B. Gong, Phys. Rev. E 88, 052920 (2013)] and the fact that these two systems can be mapped onto each other, we show that different chiral symmetry properties have remarkably different consequences. In (only) one model there can exist an arbitrary number of edge modes with 0 or π quasi-energy values accompanied by a proliferation of Dirac points, but (only) in the other model there can be counter-propagating chiral edge modes at the same boundary. Our results should be useful towards the ongoing efforts to topologically classify periodically driven systems, and should further motivate experimental studies of topological states using quantum systems under external control fields.

PACS numbers: 03.65.Vf, 05.30.Rt, 05.45.-a, 03.75.-b

* phygj@nus.edu.sg

I. INTRODUCTION

Topological states of matter in periodically driven systems have been attracting great theoretical and experimental interests [1–16]. This emerging area is relevant to new frontiers in condensed-matter physics research and in quantum control. The main features of a periodically driven quantum system are captured by its Floquet quasi-energy spectrum and the associated Floquet bands (when there is some translational invariance). As has been revealed in a number of simple model systems, Floquet bands often have remarkable topology that is absent in static systems. This is an exciting development because previously unseen topological states of matter may be realized by designing particular driving fields. To name a few, interesting results along this exciting research avenue include the generation of Floquet topological insulators [4], quantized adiabatic transport in the momentum space [5], and the generation of few or many Majorana fermionic modes in a driven quantum wire [3, 14].

Qualitatively, there are at least three fundamental reasons why a time-periodic driving field may create new or even exotic topological states of matter. The first is the winding of the quasi-energy over the quasi-energy Brillouin zone. The second is that when a driving Hamiltonian is non-perturbative, the problem under study may bear little resemblance to the undriven problem. Lastly, a periodic driving may also destroy or create new symmetry properties of the system. Interestingly, despite recent advances in this topic, a complete picture of the symmetry effects on topological states of matters in driven systems, especially on the issue of bulk-edge correspondence [17–19], is still lacking. That is, in static systems, it is well known that a non-trivial band topology should be accompanied by topologically protected edge states, with the tenfold classification scheme [20] linking the dimensionality and symmetry of a static system to its associated topological invariants and protected edge states. By contrast, the implications of different symmetries for the link between bulk Floquet band topology and the edge states in periodically driven systems are still not so clear.

The aim of this paper is to investigate some symmetry effects on edge state behavior in two periodically driven systems with nontrivial Floquet band topology. Our investigation is unique because it is the first of such efforts exploiting two systems that can be mapped onto each other. The two models are the so-called kicked Harper model (KHM) [21–32] (also regarded as a kicked quantum Hall system in Ref. [15]) and an on-resonance double-

kicked rotor (ORDKR) model [33, 34]. Both models display Hofstadter’s butterfly quasi-energy spectrum [34–36] and have played important roles in understanding the quantum dynamics in classically chaotic systems [22–29, 31, 32, 37, 38]. The topological equivalence between these two models in the bulk Floquet band topology (assisted by an additional phase parameter), as well as an explicit mapping between them, has been proven recently in those cases with an odd number of Floquet bands [39].

Given the fact that the two model systems exploited in this work can be mapped onto each other, we have here an unprecedented opportunity to understand how different symmetry properties of periodically driven systems might directly affect the edge state behavior, with the bulk eigenstates (i.e., eigenstates obtained under periodic boundary conditions) being equivalent up to a mapping in the parameter space [40]. For example, even when the two models have exactly the same Floquet band Chern numbers for the bulk spectrum, their edge state properties are still drastically different, thus reflecting a big influence of some symmetry properties on the issue of bulk-edge correspondence.

Specifically, we will show that both the KHM and the ORDKR models possess chiral symmetry (CS), but their related CS operators have different properties. These differences in their CS operators lead to a striking difference in their edge states: there are topologically protected 0 and π edge modes in the ORDKR model but not in the KHM; and there are novel counter-propagating chiral edge modes in the KHM (first found in Ref. [15]) but not in the ORDKR model. These results should be useful for the ongoing efforts to better understand topological states of matter in periodically driven systems.

We also highlight another interesting observation made from this study. In particular, it is found that in a lattice version of the ORDKR model (with an even number of bulk Floquet bands) subject to an open boundary condition, the system can host an arbitrarily large number of topologically protected edge modes with 0 or π quasi-energy values. This is accompanied by a proliferation of Dirac-like points in the quasi-energy spectrum. This might open up a new route to the simulation of Majorana modes and Dirac-like particles with the use of periodically driven systems. At the end of this paper, we also discuss in detail the possibility of experimental studies of the models analyzed here.

The outline of this paper is as follows. In Sec. II, we first introduce in detail the KHM and the ORDKR models, originally discussed in the quantum chaos literature and often addressed in the angular momentum representation. To study their edge state behaviour,

we introduce lattice implementations of these two models, which we refer to as the Kicked Harper Lattice (KHL) and the Double Kicked Lattice (DKL) models, respectively. These lattice versions, mathematically identical to the original KHM and ORDKR due to an equivalence between the lattice sites and the angular momentum representation, are physically more meaningful. We explicitly construct the CS operators for the two models in Sec. III. The difference in their edge state behaviour in the two models is made obvious by studying 2-band and 3-band examples of both models in Sec. IV and Sec. V respectively. In Sec. VI we discuss possible experimental realizations of our theoretical results. This is followed by a concluding discussion in Sec. VII.

II. TWO DYNAMICAL MODELS AND THEIR IMPLEMENTATIONS ON A LATTICE

A. Bulk properties of KHM and ORDKR

For completeness and to indicate the interdisciplinary nature of this work, this section starts with some introduction of the KHM and the ORDKR model in the context of quantum chaos. Readers who are not familiar with quantum chaos studies may skip the material here.

The KHM displays chaos (given a suitable choice of parameters) when treated classically, but its quantum version is simple enough for accurate numerical study. Insights on many topics have been gained from studies of this model. Such topics include metal-insulator transitions [25, 31, 32] and even quantum eigenstate topology [24, 30]. Remarkably, the KHM displays an unusual fractal-like quasi-energy spectrum due to its close connection [23] with the famous Hofstadter's fractal energy spectrum problem [41]. KHM studies probing the physical implications of a fractal spectrum unveiled relationships between fractality and quantum dynamics [26], quantum correlations [27] and other manifestations of quantum chaos [23]. A relatively simple realization of the KHM may be based on a kicked charge in a magnetic field [21, 29].

The ORDKR model, a particular version of modulated kicked rotors [42], is another dynamical model which has yielded interesting physics [33]. It has been found to display intriguing features such as ratchet acceleration [38] and exponential quantum spreading [37]. Intriguingly, under an appropriate choice of parameters, the ORDKR has been found to dis-

play a Hofstadter-like quasi-energy spectrum that is much analogous to that of the KHM [34, 35] while at the same time displaying qualitatively different dynamics [34]. Subsequent work [36] found that the spectra of the two models are identical provided that either an effective Planck constant parameter is irrational or a union of spectra over an added phase shift parameter (as seen later, this phase shift parameter may be taken as the crystal momentum along the second dimension of a two dimensional (2D) “ancestor” model) is taken in both models. In a very recent work [39], it was further shown that the modified KHM and ORDKR with the added phase shift parameter both host topologically non-trivial quasi-energy bands evidenced by nonzero Chern numbers (defined with respect to a Bloch phase and the additional phase shift parameter). The topologically nontrivial Floquet bands in both models display many interesting topological phase transitions. Most importantly, the work of [39] found that, in cases with an odd number of bands, the two models must display exactly the same Chern numbers so long as certain parameters in one system are equal to corresponding parameters in the other [40]. These Chern numbers were found in our previous work [5] to describe the average momentum gained by special (Wannier) initial states after the phase shift parameter has been tuned adiabatically over one cycle.

B. Lattice implementations of KHM and ORDKR

The vast literature about KHM and our recent studies of ORDKR are based on angular momentum representation and both models form continuous Floquet bands due to a translational invariance in the angular momentum space. This is not convenient for the investigation of bulk-edge correspondence because it is not clear how to introduce a physical boundary in the angular momentum space. For that reason we shall consider lattice versions of ORDKR and KHM.

We consider a 2-dimensional (2D) square lattices of $L_x \times L_y$ sites. Throughout this paper, we shall always consider periodic boundary conditions along y (one can also assume at the same time that the y dimension is not bounded). To study the issue of bulk-edge correspondence, we will consider in turn both open and periodic boundary conditions along x . We denote by $|n_{x(y)}\rangle$ the discrete lattice sites along x (y), where $n_{x(y)} = 0, \dots, L_{x(y)} - 1$ [46]. An arbitrary state in the Hilbert space is then written as $|\psi\rangle = \sum_{n_x, n_y} \psi_{n_x, n_y} |n_x\rangle |n_y\rangle$.

1. DKL as a lattice version of ORDKR

The first model we consider is a double-kicked lattice (DKL) model [43, 44], a lattice version of ORDKR, described by the following Hamiltonian:

$$H_{\text{DKL}}(t) = V(t)\hat{n}_x^2 + \frac{1}{2} \sum_{n_x=0}^{L_x-1} \left(\hat{J}(t) |n_x + 1\rangle \langle n_x| + \hat{J}^\dagger(t) |n_x\rangle \langle n_x + 1| \right), \quad (1)$$

with

$$\begin{aligned} V(t) &= 0; & \hat{J}(t) &= J_1 \sum_{n_y=0}^{L_y-1} |n_y + 1\rangle \langle n_y| & \text{for } 4m \leq t < 4m + 1, \\ V(t) &= V; & J(t) &= 0 & \text{for } 4m + 1 \leq t < 4m + 2, \\ V(t) &= 0; & J(t) &= J_2 & \text{for } 4m + 2 \leq t < 4m + 3, \\ V(t) &= -V; & J(t) &= 0 & \text{for } 4m + 3 \leq t < 4(m + 1), \end{aligned} \quad (2)$$

where $m \in \mathbb{Z}$. The above Hamiltonian describes a time-periodic protocol consisting of four stages per period. During the first stage, the Hamiltonian describes a particle undergoing hopping in a diagonal fashion on the lattice. In the second stage, the particle is subject to a potential of strength V which is quadratic along x and independent of y . Next, the particle experiences a nearest-neighbour hopping of strength $J_2/2$ along only the x -direction. Finally, the particle experiences again the same potential that is quadratic along x , except with negative strength $-V$, meaning that this parabolic potential is inverted relative to the earlier one. The consideration of a finite lattice (i.e., open boundary conditions) will reveal edge state properties, whereas applying periodic boundary conditions will reveal the bulk spectrum. For the latter purpose, we may obtain a compact form of the Floquet operator for the DKL, by introducing the translationally invariant crystal momentum states, defined by

$$|k_{x(y)}\rangle = \frac{1}{\sqrt{L_{x(y)}}} \sum_{n_{x(y)}=0}^{L_{x(y)}-1} |n_{x(y)}\rangle e^{-ik_{x(y)}n_{x(y)}} \quad (3)$$

along $x(y)$, where $k_{x(y)} = -\pi + j \times 2\pi/L_{x(y)}$ and $j = 0, 1, \dots, L_{x(y)} - 1$. Using the above equation, one may show that the Floquet operator which propagates from $t = 0$ to $t = 4$ takes the form

$$U_{\text{DKL}}(J_2, V, J_1) = e^{i\hat{n}_x^2 V} e^{-iJ_2 \cos(\hat{k}_x)} e^{-i\hat{n}_x^2 V} e^{-iJ_1 \cos(\hat{k}_x + \hat{k}_y)}, \quad (4)$$

where we have chosen to work in dimensionless units such that $\hbar = 1$. The above U_{DKL} is seen to be of precisely the same form as the Floquet operator of an ORDKR treated in the angular momentum space [34], with \hat{n}_x playing the role of the angular momentum operator and \hat{k}_x playing the role of an angular variable, and \hat{k}_y playing the role of a phase shift parameter.

Throughout, we denote the quasi-energy and the associated eigenstate of a Floquet operator U as ω_n and $|\psi_n\rangle$ [45], with $\hat{U}|\psi_n\rangle = e^{-i\omega_n}|\psi_n\rangle$. Since the quasi-energy is only defined modulo 2π , we define the quasi-energy Brillouin zone (BZ) as ranging from $-\pi$ to π . By choosing V such that $V = \pi M/N$, where $M, N \in \mathbb{Z}$, then the Floquet operator U_{DKL} becomes periodic in the $|n_x\rangle$ representation with period N . Bloch's theorem then yields that we will have a quasi-energy spectrum consisting of N bands. For low values of $J_{1,2}$, the spectrum consists of N bands separated by large gaps. For a fixed value of V , increasing the values of $J_{1,2}$ will cause the quasi-energy bands to broaden and occupy more space within the BZ. As $J_{1,2}$ increase beyond certain special values, the quasi-energy bands will touch and re-separate, possibly causing a topological phase transition. Later, we shall study the spectra obtained as $J_{1,2}$ increase for different $V = \pi M/N$ and observe the effects that the topological phase transitions have on the topological invariants and related edge states.

2. KHL as a lattice version of KHM

Here we consider a lattice version of KHM, which we refer to as the kicked Harper lattice (KHL), described by Hamiltonian

$$\begin{aligned} H_{\text{KHL}}(J, R, b) &= \frac{J}{2} \sum_{n_x=0}^{L_x-1} (|n_x+1\rangle\langle n_x| + |n_x\rangle\langle n_x+1|) + \\ &\quad \frac{R}{2} \sum_{n_x, n_y=0}^{L_x-1, L_y-1} (e^{in_x b} |n_x, n_y\rangle\langle n_x, n_y+1| + \text{h.c.}) \sum_m \delta(t-m) \\ &= J \cos(\hat{k}_x) + R \cos(\hat{n}_x b - \hat{k}_y) \sum_m \delta(t-m), \end{aligned} \quad (5)$$

with $m \in \mathbb{Z}$, where we have made use of Eq. (3) in order to obtain the second line that applies to the case under periodic boundary condition (for the purpose of understanding the bulk spectrum). The above Hamiltonian is directly related to a solid-state system subject to a kicking control field and in [15] it was called a kicked Hall system. The Floquet operator

evolving states from time $t = 0^+$ to time $t = 1^+$ is then given by

$$U_{\text{KHL}}(J, R, b) = e^{-iR \cos(\hat{n}_x b - \hat{k}_y)} e^{-iJ \cos(\hat{k}_x)}. \quad (6)$$

Once again, it is seen that this form is indeed the familiar form of the Floquet operator of KHM, with \hat{k}_y playing the role of a phase shift parameter, as introduced in our early studies [36, 38, 39]. This finishes our construction of the lattice versions of ORDKR and KHM.

III. CONSTRUCTION OF CHIRAL SYMMETRY OPERATORS

The work of [2] suggested that given a Floquet operator \hat{U} , assuming that there is no winding of quasi-energy across the BZ seen in the bulk spectrum (i.e., the spectrum is obtained under periodic boundary conditions), one may extract an effective static Hamiltonian, \hat{H}_{eff} , via the relation

$$\hat{U} \equiv e^{-i\hat{H}_{\text{eff}}}, \quad (7)$$

and classify \hat{H}_{eff} according to the tenfold classification scheme for static systems [20], thus effectively classifying \hat{U} . Following this approach, a Floquet operator \hat{U} is said to possess chiral symmetry (CS) [2, 10, 20] if there exists a unitary and Hermitian operator Γ such that

$$\Gamma \hat{U} \Gamma^\dagger = \hat{U}^{-1}, \quad (8)$$

with Γ obeying $\Gamma^2 = \mathbb{1}$ [2, 10]. We shall refer to Γ as the CS operator. We follow this approach in an attempt to topologically classify the DKL and KHL Floquet operators. An ambiguity naturally arises at this point. Namely, there is an arbitrary choice of which one-period time frame to choose for a Floquet operator to propagate across. It turns out, however, that different choices can lead to \hat{H}_{eff} obeying different symmetries. We follow the strategy introduced in [10] and seek “symmetric time frames”, which are defined as choices of time frames resulting in Floquet operators \hat{U} of the form

$$\hat{U} = \hat{F} \hat{G}, \quad (9)$$

where \hat{F} and \hat{G} are unitary operators related with each other and the CS operator via

$$\Gamma \hat{F} \Gamma = \hat{G}^{-1}. \quad (10)$$

It is trivial to prove that once this relation is obeyed, the CS condition in Eq. (8) is necessarily also obeyed. Such symmetric time frames do not exist for arbitrary Floquet operators but are found to exist in the DKL and KHL. It is easy to see that if a symmetric time frame exists corresponding to a Floquet operator $\hat{U}' = \hat{F}\hat{G}$ exists, then there must also be a second symmetric time frame corresponding to Floquet operator $\hat{U}'' = \hat{G}\hat{F}$ [10].

A. Chiral symmetry operator for DKL

The Floquet operator for the DKL model in a symmetric time frame from $t = 2.5$ to $t = 6.5$ (cf. Eqs. (1) and (2)) reads

$$U'_{\text{DKL}}(J_2, V, J_1) = e^{-i\frac{J_2}{2}\cos(\hat{k}_x)}e^{-i\hat{n}_x^2V}e^{-iJ_1\cos(\hat{k}_x+\hat{k}_y)}e^{i\hat{n}_x^2V}e^{-i\frac{J_2}{2}\cos(\hat{k}_x)}, \quad (11)$$

where

$$\begin{aligned} \hat{F} &\equiv e^{-iJ_2\cos(\hat{k}_x)/2}e^{-i\hat{n}_x^2V}e^{-iJ_1\cos(\hat{k}_x+\hat{k}_y)/2} \\ \hat{G} &\equiv e^{-iJ_1\cos(\hat{k}_x+\hat{k}_y)/2}e^{i\hat{n}_x^2V}e^{-iJ_2\cos(\hat{k}_x)/2}. \end{aligned} \quad (12)$$

The CS operator is given by

$$\Gamma_{DK} = e^{i\hat{n}_x\pi}. \quad (13)$$

It is clear that

$$\Gamma_{\text{DK}}^2 = 1 \quad (14)$$

and

$$\Gamma_{\text{DK}} = \Gamma_{\text{DK}}^\dagger = \Gamma_{\text{DK}}^{-1} \quad (15)$$

since \hat{n}_x has only integer eigenvalues. Making use of the fact that

$$e^{i\hat{n}_x\pi}f(\hat{k}_x)e^{-i\hat{n}_x\pi} = f(\hat{k}_x + \pi) \quad (16)$$

for an arbitrary function f , we see that

$$\begin{aligned} \Gamma_{\text{DK}}U'_{\text{DKL}}\Gamma_{\text{DK}} &= \Gamma_{\text{DK}}\hat{F}\hat{G}\Gamma_{\text{DK}} \\ &= \Gamma_{\text{DK}}\hat{F}\Gamma_{\text{DK}}^2\hat{G}\Gamma_{\text{DK}} \\ &= \hat{G}^{-1}\hat{F}^{-1} \\ &= U'^{-1}_{\text{DKL}}. \end{aligned} \quad (17)$$

In other words, the DKL Floquet operator possesses chiral symmetry in a symmetric time frame. Interestingly, for Floquet operators of the DKL model corresponding to arbitrary (non-symmetric) time frames, there do *not* exist in general such CS operators satisfying the CS condition. This fact might hint at the existence of some generalized form of chiral symmetry or topological protection which exists in all the Floquet operators regardless of the choice of time-frame. If such a generalization exists, it has yet to be found.

B. Chiral symmetry operator for KHL

Here we analyse the symmetry of the KHL Floquet operator constructed above. Defining the Floquet operator as propagating states across the symmetric time frame from $t = 0.5$ to $t = 1.5$ (cf. Eq. (5)), we obtain

$$U'_{\text{KHL}}(J, R, b) = e^{-i\frac{J}{2}\cos(\hat{k}_x)} e^{-iR\cos(\hat{n}_x b - \hat{k}_y)} e^{-i\frac{J}{2}\cos(\hat{k}_x)}. \quad (18)$$

The CS operator of the above model is given by

$$\Gamma_{\text{KH}} = e^{i\hat{n}_x\pi} e^{i\hat{n}_y\pi}. \quad (19)$$

Clearly,

$$\Gamma_{\text{KH}}^2 = \mathbb{1} \quad (20)$$

and

$$\Gamma_{\text{KH}} = \Gamma_{\text{KH}}^{-1} = \Gamma_{\text{KH}}^\dagger. \quad (21)$$

The CS condition may be easily verified using Eq. (16) as follows.

$$\begin{aligned} & \Gamma_{\text{KH}} e^{-i\frac{J}{2}\cos(\hat{k}_x)} e^{-iR\cos(\hat{n}_x b - \hat{k}_y)} e^{-i\frac{J}{2}\cos(\hat{k}_x)} \Gamma_{\text{KH}} \\ &= e^{-i\frac{J}{2}\cos(\hat{k}_x + \pi)} e^{-iR\cos(\hat{n}_x b - (\hat{k}_y + \pi))} e^{-i\frac{J}{2}\cos(\hat{k}_x + \pi)} \\ &= e^{i\frac{J}{2}\cos(\hat{k}_x)} e^{iR\cos(\hat{n}_x b - \hat{k}_y)} e^{i\frac{J}{2}\cos(\hat{k}_x)} \\ &= U'^{-1}_{\text{KHL}}(J, R, b). \end{aligned} \quad (22)$$

Thus, the presence of CS in the KHL model is explicitly verified. Similar to the DKL model, if we choose $b = 2\pi \times M/N$ in the KHL model, this results in a quasi-energy spectrum of N bands. We may then tune the values of J and R to induce topological phase transitions and study the behaviour of the topological invariants and edge states. We note that the CS

operator of the KHL is not diagonal in k_y , a feature different from that of the DKL. This fact will be important later. Lastly, we note also that for both models, it can be shown that the CS condition of Eq. (8) is still obeyed even under the open boundary condition along the x dimension.

We have thus proven that the Floquet operators for both models possess chiral symmetry, at least within certain time frames, and have identified their CS operators. Next, we will investigate the band structure of the two models for different V and b values. In particular, we will investigate the band structure under open boundary conditions along x and study the issue of bulk-edge correspondence of the two models in the 2-band and 3-band cases. We will find that due to the particular forms of the CS operators of the two models, their edge states will be drastically different in spite of a direct mapping between the two models.

IV. EFFECTS OF SYMMETRY IN 2-BAND CASES

A. Existence or nonexistence of topological protection for 0 and π edge modes

Here, we study the case where $V = \pi/2$ in Eq. (11) and $b = \pi$ in Eq. (18), corresponding to 2-band spectra. To study the existence of edge modes, we adopt open boundary conditions along the x direction in both models, with lattice sites $n_x = 0, 1, \dots, L_x - 1$, and using periodic boundary conditions only along y . Since both Floquet operators are clearly diagonal in the crystal momentum along y (i.e., \hat{k}_y) we may replace the operator \hat{k}_y in the Floquet operators with its eigenvalue k_y , bearing in mind that this assumes that the y -component of the state acted upon by the Floquet operator is $|k_y\rangle$. In other words,

$$U'_{\text{KHL}} = \sum_{k_y} U'_{\text{KHL}}(k_y) \otimes |k_y\rangle \langle k_y|; \quad (23)$$

$$U'_{\text{DKL}} = \sum_{k_y} U'_{\text{DKL}}(k_y) \otimes |k_y\rangle \langle k_y|. \quad (24)$$

The $U'_{\text{KHL}}(k_y)$ and $U'_{\text{DKL}}(k_y)$ operators may be interpreted as 1D “descendents” of the 2D Floquet operators U'_{KHL} and U'_{DKL} . Note that for convenience, we use the same notation for the Floquet operators as before, though we use the open boundary condition along the x dimension and carry out the calculations for the respective Floquet operators numerically.

With all these conditions in place, we numerically diagonalize the two 1D descendent Floquet operators over a large range of $J_{1,2}$, J and R values as a function of k_y . Remarkably,

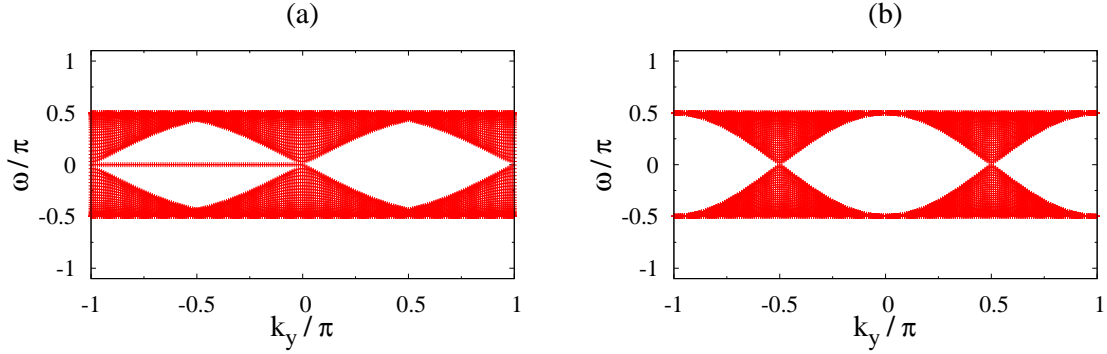


FIG. 1. (color online). The QE spectra for (a) the double-kicked lattice model for $V = \pi/2$, $J_1 = J_2 = 0.5\pi$ and (b) the kicked Harper lattice model for $b = \pi$, $R = J = 0.5\pi$ under open boundary conditions along x . It is clear that topologically protected 0 modes appear only in the former case.

we find that the DKL model hosts 0 and π edge modes while the KHL model does not. An illustrative example is shown in Fig. 1, where the edge modes with 0 quasi-energy value in the DKL case are seen, which is plotted as the middle flat line in the left panel.

Interestingly, one may turn to the specific form of the CS operators for both models to explain the observed difference in edge states. In the case of the DKL, the CS operator Γ_{DK} relates $U'_{\text{DKL}}(k_y)$ to $U'^{\dagger}_{\text{DKL}}(k_y)$. On the other hand, in the case of the KHL, the different CS operator Γ_{KH} relates $U'_{\text{KHL}}(k_y)$ to $U'^{\dagger}_{\text{KHL}}(k_y + \pi)$. This stems from the fact that Γ_{KH} has less translational symmetry than the KHL Floquet operator, whereas Γ_{DK} has the same translational symmetry as the DKL Floquet operator (ie. periodic along y over every 1 lattice site). For a detailed derivation of these properties of the CS operators, see Appendix A.

Given this difference in their CS operators, one may explain the robustness of the $\omega = 0$ and π quasi-energy modes in the DKL model as follows: so long as CS is maintained, if there exists an eigenstate with quasi-energy ω at some k_y , there must also exist an eigenstate with quasi-energy $-\omega$ at *the same* k_y . For $\omega = 0$ (or π) quasi-energies, these quasi-energies could correspond to one and the same eigenstate (note that π and $-\pi$ are the same in the quasi-energy BZ). Hence, if at some k_y there is a single eigenstate with quasi-energy $\omega = 0$ (π) within a gap, this state is not allowed to have its quasi-energy move away from 0 (π) under any CS-preserving perturbation [7] for the simple reason that a single state

cannot suddenly split into two under continuous change of parameters. This constitutes a topological protection of *single* 0 and π quasi-energy edge states in the DKL model. A proof that not just one but multiple such edge states may be robust in the DKL model is provided in Appendix A.

The situation is rather different for U'_{KHL} , i.e., a kicked quantum Hall system under open boundary conditions along x . In this case, if there exists an eigenstate with quasi-energy ω at some k_y , then the CS condition requires that there must also exist an eigenstate with quasi-energy $-\omega$ at $k_y + \pi$. In other words, the chiral symmetry partner lies at a *different* value of k_y and is thus guaranteed to be a distinct eigenstate. Hence, the presence of CS here does not offer a mechanism towards a topological protection of states with quasi-energies 0 or π .

B. Topological invariants for the bulk spectrum of DKL

To further understand the connection between the 0 and π quasi-energy edge modes and the bulk spectrum, we follow a procedure [10] originally used in the context of quantum random walks to derive the topological invariants in the presence of CS. To that end, we first write the two operators in a more suitable form. Taking periodic boundary conditions along x and y , we divide the 1D lattice space $\{|n_x\rangle\}$ as before into the sublattices A and B. Each sublattice is of size $S \equiv L_x/2$. We set L_x to be a multiple of 4 for convenience (i.e., so that we have an even number of unit cells S). We denote the sites of sublattice A as $|j, A\rangle \equiv |n_x = 2j\rangle$, and the sites of sublattice B as $|j, B\rangle \equiv |n_x = 2j + 1\rangle$ where $j = 0, \dots, S - 1$. We then define the reciprocal lattices of $|j, A(B)\rangle$ via the Discrete Fourier Transform as

$$|\bar{k}_x, A(B)\rangle = \frac{1}{\sqrt{S}} \sum_j |j, A(B)\rangle e^{-ij\bar{k}_x}, \quad (25)$$

where $\bar{k}_x = -\pi, -\pi + 2\pi/S, \dots, \pi - 2\pi/S$. We have chosen to denote the quasimomentum as \bar{k}_x to make it clear that it corresponds to the space of states $|\bar{k}_x\rangle$ which are Bloch-periodic (ie. periodic up to a phase factor) in the lattice space over every 2 sites and is not the same as the k_x seen earlier which corresponds to states which are Bloch-periodic over every 1 site.

Using Eq. (25) to write $U'_{\text{DKL}}(k_y)$ in $|\bar{k}_x\rangle$ representation, we obtain

$$\begin{aligned} U'_{\text{DKL}}(k_y) &\equiv e^{-i \sum_{\bar{k}} H'_{\text{eff}}(\bar{k}_x) \otimes |\bar{k}_x\rangle \langle \bar{k}_x|}, \\ &= \sum_{\bar{k}_x} e^{-i H'_{\text{eff}}(\bar{k}_x)} \otimes |\bar{k}_x\rangle \langle \bar{k}_x|, \end{aligned} \quad (26)$$

where

$$H'_{\text{eff}}(\bar{k}_x) = \mathbf{h}'(\bar{k}_x) \cdot \sigma \quad (27)$$

is a 2×2 matrix describing transitions within the reciprocal sublattice index degree of freedom. That is $(H')_{1,1}$ [or $(H')_{2,2}$] describes transitions from the $|\bar{k}_x, A\rangle$ [or $|\bar{k}_x, B\rangle$] state back onto itself, while $(H')_{1,2}$ [or $(H')_{2,1}$] describes transitions from $|\bar{k}_x, B\rangle$ [or $|\bar{k}_x, A\rangle$] to $|\bar{k}_x, A\rangle$ [or $|\bar{k}_x, B\rangle$]. The explicit form of $U'_{\text{DKL}}(k_y)$ in \bar{k}_x representation and its effective Hamiltonian are given as follows.

$$U'_{\text{DKL}}(k_y) \equiv e^{-i \sum_{\bar{k}_x} H'_{\text{eff}}(\bar{k}_x, k_y) \otimes |\bar{k}_x\rangle \langle \bar{k}_x|}, \quad (28)$$

where

$$\begin{aligned} H'_{\text{eff}}(\bar{k}_x, k_y) &= \mathbf{h}'(\bar{k}_x, k_y) \cdot \sigma, \\ \mathbf{h}'(\bar{k}_x, k_y) &= E(\bar{k}_x, k_y) \mathbf{n}'(\bar{k}_x, k_y), \\ E(\bar{k}_x, k_y) &= \cos^{-1} [\cos(P) \cos(Q)], \\ \mathbf{n}'(\bar{k}_x, k_y) &= [n'_x(\bar{k}_x, k_y), n'_y(\bar{k}_x, k_y), 0], \\ n'_x(\bar{k}_x, k_y) &= \frac{\cos(\frac{\bar{k}_x}{2}) \sin(P) \cos(Q) - \sin(\frac{\bar{k}_x}{2}) \sin(Q)}{\sin(E(\bar{k}_x, k_y))}, \\ n'_y(\bar{k}_x, k_y) &= \frac{-\sin(\frac{\bar{k}_x}{2}) \sin(P) \cos(Q) - \cos(\frac{\bar{k}_x}{2}) \sin(Q)}{\sin(E(\bar{k}_x, k_y))}, \\ P &\equiv J_2 \cos\left(\frac{\bar{k}_x}{2}\right), \\ Q &\equiv J_1 \cos\left(k_y + \frac{\bar{k}_x}{2}\right). \end{aligned} \quad (29)$$

Note that $|\mathbf{n}'(\bar{k}_x)| = 1$. The bulk quasi-energies are then given by $\pm E(\bar{k}_x, k_y)$. The fact that $\mathbf{h}'(\bar{k}_x, k_y)$ for a fixed k_y always resides in the $x - y$ plane as \bar{k}_x is tuned is consistent with the form of the CS operator of the DKL Floquet operator written in the \bar{k}_x representation, which reads as

$$\begin{aligned} \Gamma_{\text{DK}} &= \sum_{\bar{k}_x} e^{-i \frac{\pi}{2}} e^{i \frac{\pi}{2} \sigma_z} \otimes |\bar{k}_x\rangle \langle \bar{k}_x| \otimes \sum_{k_y} |k_y\rangle \langle k_y| \\ &\equiv \Gamma_{\text{DK}}^{(x)} \otimes \sum_{k_y} |k_y\rangle \langle k_y|, \end{aligned} \quad (30)$$

where

$$\Gamma_{\text{DK}}^{(x)} \equiv \sum_{\bar{k}_x} e^{-i\frac{\pi}{2}} e^{i\frac{\pi}{2}\sigma_z} \otimes |\bar{k}_x\rangle \langle \bar{k}_x|. \quad (31)$$

This form of $\Gamma_{\text{DK}}^{(x)}$ shows that it performs a rotation of all the $\mathbf{h}'(\bar{k}_x, k_y)$ vectors by an angle of π about the z -axis. We also note that the fact that $\Gamma_{\text{DK}}^{(x)}$ performs a π -rotation about z and $\mathbf{h}'(\bar{k}_x, k_y)$ lies purely in the $x - y$ plane together imply that

$$\Gamma_{\text{DK}}^{(x)} \mathbf{h}'(\bar{k}_x, k_y) \Gamma_{\text{DK}}^{(x)\dagger} = -\mathbf{h}'(\bar{k}_x, k_y), \quad (32)$$

which we can be also directly checked using Eq. (A1).

As we mentioned during the construction of CS operators in Sec. III, we may also consider a second symmetric time frame, in which the Floquet operator is denoted as U''_{DKL} . We can then define $U''_{\text{DKL}}(k_y)$ in the $|\bar{k}_x\rangle$ representation just as we did for $U'_{\text{DKL}}(k_y)$:

$$U''_{\text{DKL}}(k_y) = \sum_{\bar{k}} e^{-iH''_{\text{eff}}(\bar{k}_x)} \otimes |\bar{k}_x\rangle \langle \bar{k}_x|, \quad (33)$$

with

$$H''_{\text{eff}}(\bar{k}_x) = \mathbf{h}''(\bar{k}_x) \cdot \sigma. \quad (34)$$

The explicit form of $\mathbf{h}''(\bar{k}_x)$ is given in Appendix B. We need only note here that $\mathbf{h}'(\bar{k}_x)$ and $\mathbf{h}''(\bar{k}_x)$ always lie in the same plane (in this case the $x - y$ plane) for all values of \bar{k}_x , which is to be expected since they share the same CS operator. This allows one to define the winding numbers ν' and ν'' of $H'_{\text{eff}}(\bar{k}_x)$ and $H''_{\text{eff}}(\bar{k}_x)$ respectively. These winding numbers count the number of times the \mathbf{h} vector encircles the origin as \bar{k}_x is scanned across its Brillouin zone from $-\pi$ to π . The standard bulk-edge correspondence result for such winding numbers [10, 20] gives that the total number of edge states localized at a boundary between two bulks with winding numbers ν_L and ν_R (“L” for left, “R” for right) is equal to the absolute value of the difference $\nu_L - \nu_R$. Applying this result to our case, we obtain

$$\nu'_L - \nu'_R = m'_{A,0} + m'_{A,\pi} - m'_{B,0} - m'_{B,\pi} \quad (35)$$

for the first (single-prime) symmetric time frame and

$$\nu''_L - \nu''_R = m''_{A,0} + m''_{A,\pi} - m''_{B,0} - m''_{B,\pi} \quad (36)$$

in the second (double-prime) symmetric time frame. Here $m_{A,0}$ and $m_{A,\pi}$ ($m_{B,0}$ and $m_{B,\pi}$) refer to the number of edge states with 0 and π quasi-energy values respectively for sublattice

A (for sublattice B). In our extensive numerical results, these relations are found to hold always.

In Appendix C, we follow Ref. [10] and are able to show that the $\omega = 0$ edge states in the two symmetric frames live on the same sublattice, while the $\omega = \pi$ edge states in the two symmetric frames live on different sublattices. This leads to

$$\begin{aligned} m'_{A,0} &= m''_{A,0}, & m'_{A,\pi} &= m''_{B,\pi}, \\ m'_{B,0} &= m''_{B,0}, & m'_{B,\pi} &= m''_{A,\pi}. \end{aligned} \quad (37)$$

Combining Eqs. (37) with Eqs. (35) and (36), one has

$$m'_{A,0} - m'_{B,0} = \frac{\nu'_L + \nu''_L}{2} - \frac{\nu'_R + \nu''_R}{2}, \quad (38)$$

$$m'_{A,\pi} - m'_{B,\pi} = \frac{\nu'_L - \nu''_L}{2} - \frac{\nu'_R - \nu''_R}{2}. \quad (39)$$

This relation, first discovered in [10], reveals that the bulk topological invariant governing the number of topologically protected 0 and π modes are $\nu_0 \equiv (\nu' + \nu'')/2$ and $\nu_\pi \equiv (\nu' - \nu'')/2$ respectively. In other words, the number of topologically protected edge modes with 0 quasi-energy at the boundary is

$$m'_{A,0} - m'_{B,0} = \nu_{0,L} - \nu_{0,R}, \quad (40)$$

while the number of protected edge modes with π quasi-energy at the boundary is

$$m'_{A,\pi} - m'_{B,\pi} = \nu_{\pi,L} - \nu_{\pi,R}. \quad (41)$$

We consider again a system with open boundaries along x as we did earlier. The above relations give the number of protected 0 and π quasi-energy modes at the boundaries of such a system in terms of bulk invariants (i.e., defined under periodic boundary conditions). Focusing on the right boundary, the left (L) bulk is the DKL model and the right (R) bulk is the vacuum. In this case, $\nu_{0,R} = \nu_{\pi,R} = 0$ (the vacuum may be regarded as a particular bulk with winding number 0) and the 0 and π edge modes are given simply by the winding numbers ν_0 and ν_π of the driven lattice's effective Hamiltonian. Such a bulk-edge correspondence via the topological invariants ν_0 and ν_π has been extensively verified in our numerical studies (many results are not shown here).

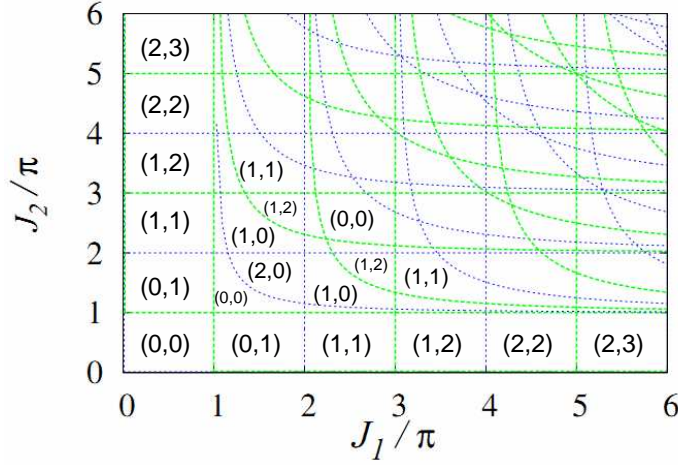


FIG. 2. (color online). Phase transition lines of the DKL model in the (J_1, J_2) space for $k_y = \pi/2$. Gap closures at $\omega = 0(\pi)$ are marked with a blue-dashed (green-dashed). The (ν_0, ν_π) numbers signifying the number of 0 and π modes respectively at each edge (under open boundary conditions) are indicated within each region of the parameter space. Note that the number of edge modes seems to increase indefinitely when we fix J_1 (J_2) at 0.5π and increase J_2 (J_1).

C. Topological phase diagram of the DKL

With the bulk-edge correspondence of the DKL thoroughly formulated, we may now explore the behaviour of the bulk invariants as we tune the system parameters. To that end, we present in Fig. 2 below the values of (ν_0, ν_π) at $k_y = \pi/2$ over a large range of (J_1, J_2) values of the DKL model. In fact, the topological phase diagrams for all other $k_y \neq 0, \pi$ can be easily obtained and are found to be similar to Fig. 2, differing only by some shifts of the transition lines. The shown topological phase diagram is seen to possess a wide variety of different topological phases. In particular, for fixed $J_1 = \pi/2$ (but any $0 < J_1 < \pi$ will also suffice), as we increase the value of J_2 , we will pass through alternate gap closures at $\omega = 0$ and $\omega = \pi$. With each of these closures, ν'' increases by 1 while ν' alternates between -1 and 0. This pattern seems to carry on ad infinitum, meaning that the number of $\omega = 0$ and $\omega = \pi$ topologically protected edge modes at each boundary with the vacuum, given by $\nu_0 = (\nu' + \nu'')/2$ and $\nu_\pi = (\nu' - \nu'')/2$ respectively, will become very large as J_2 becomes large. A similar situation happens if we fix $J_2 = \pi/2$ and increase J_1 .

An especially interesting feature is that, as we can see from Fig. 2, the phase transition lines do not occupy the parameter space densely along the $J_1 = 0.5\pi$ ($J_2 = 0.5\pi$) line no matter large J_2 (J_1) becomes, unlike in the regions in the upper right corner of Fig. 2 where the phase transition lines become increasingly dense as both J_1 and J_2 increase to large values. This suggests that along these special lines in parameter space, the quasi-energy gaps will be present even if J_1 and J_2 are in practice slightly shifted due to experimental limitations. Hence, the model may be very useful for situations where one might wish to realize an arbitrarily large number of topologically protected edge modes. They will all be robust to disorder and unintentional perturbations due to the relatively robust gap. In addition, a look at Eq. (2) reveals that all one needs to do in order to effectively increase J_1 or J_2 in U'_{DKL} is to increase the two time intervals during which $J(t) \neq 0$, an experimentally rather straightforward task.

D. Proliferation of Dirac-like points in the spectrum of DKL

So what are the other implications of the topological phase diagram shown in the previous subsection? Let us now return to the DKL under the open boundary condition. We display in Fig. 3 an interesting multiplication of Dirac-like points as J_2 increases with J_1 fixed at 0.5π (note also the π quasi-energy edge modes together with the 0 quasi-energy edge modes). Consider what happens when a phase transition line of the form $J_2 = (2m + 1)\pi, m \in \mathbb{Z}$ is crossed. When $J_2 = (2m + 1)\pi$, a new Dirac-like point forms at $k_y = \pm 0.5\pi, \omega = \pi$. As J_2 increases further, the two Dirac-like points do not vanish. Instead, each Dirac-like point splits into two and moves off to either side. Hence, we now have four more Dirac-like points than we did before crossing the phase transition line. A similar sequence of event occurs when a $J_2 = 2m\pi, m \in \mathbb{Z}$ line is crossed. New Dirac-like points form at $k_y = \pm 0.5\pi, \omega = 0$ when $J_2 = 2m\pi$ and split off into two upon further increase of J_2 , again resulting in the presence of four more Dirac-like points than before the phase transition line was crossed. Hence, as J_2 is increased along the line $J_1 = 0.5\pi$, the number of Dirac-like points increases rapidly.

The above situation is similar to that reported in [47], in which it was found that as one increases the hopping range within a honeycomb graphene-like lattice model, one sees a proliferation of Dirac points accompanied by the existence of large Chern number phases.

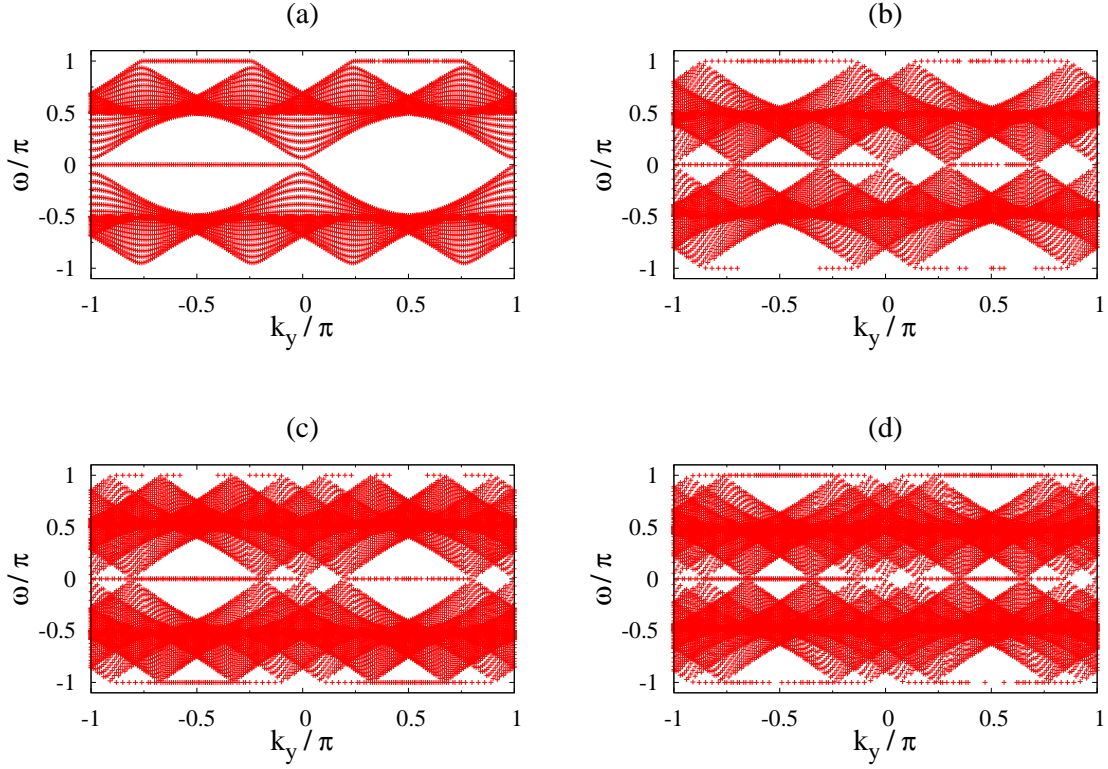


FIG. 3. (color online). The QE spectra for the DKL model as a function of k_y at $V = \pi/2$, $J_1 = 0.5\pi$, and (a) $J_2 = 1.5\pi$, (b) $J_2 = 2.5\pi$, (c) $J_2 = 3.5\pi$, (d) $J_2 = 4.5\pi$. We see a proliferation of Dirac-like points at $\omega = 0$ and $\omega = \pm\pi$ as J_2 increases.

But here it is seen to be possible to synthesize many Dirac-like points by applying a driving field to a simple lattice system.

To understand the emergence of many Dirac points, we may adopt a perspective similar to that in Ref. [14]. As we increase J_2 (or J_1), the hopping range within the effective Hamiltonian of U'_{DKL} is also increased. Indeed, the effective Hamiltonian is defined via

$$U_{\text{DKL}} \equiv e^{-i\hat{H}_{\text{eff}}}. \quad (42)$$

The Floquet operator is given by the concatenation of four exponential operators as seen in Eq. (4). Each exponential operator does not commute with the exponential operator on either side of it. Hence, in order to obtain \hat{H}_{eff} , one must apply the Baker-Campbell-Hausdorff (BCH) formula to each pair of adjacent exponential operators repeatedly until we finally are left with only one exponential operator. Now, by making use of the BCH formula,

we see that given three arbitrary operators \hat{X}, \hat{Y} and \hat{Z} related via

$$e^{-i\hat{Z}} \equiv e^{-ic_1\hat{X}}e^{-ic_2\hat{Y}}, \quad (43)$$

where c_1, c_2 are c-numbers, the operator \hat{Z} is given by

$$\hat{Z} = c_1\hat{X} + c_2\hat{Y} - \frac{ic_1c_2}{2}[\hat{X}, \hat{Y}] - \frac{c_1c_2}{12}[c_1\hat{X} - c_2\hat{Y}, [\hat{X}, \hat{Y}]] + \dots \quad (44)$$

Due to the infinite series of nested commutators of \hat{X} and \hat{Y} , we see that \hat{Z} may contain terms of longer-range hopping than those present in both \hat{X} and \hat{Y} individually. The larger the values of c_1 and c_2 , the more nested commutator terms will play a significant role in \hat{Z} . Applying this in the context of the problem at hand, we conclude that \hat{H}_{eff} will contain longer-range hopping terms beyond the nearest-neighbour hopping terms seen in Eq. (1). Larger values of J_1 and J_2 will then lead to longer-range hopping in \hat{H}_{eff} . As we saw earlier, the Floquet operator of the DKL model possesses chiral symmetry regardless of the values of J_1 and J_2 . Hence, by increasing these values, we are able to simulate an effective chiral symmetric Hamiltonian with very long-range hopping. We stress again that we simply need to increase the time interval during which the hopping is switched on to increase the hopping range of the effective Hamiltonian. This is much simpler than trying to engineer actual static Hamiltonians with long-range hopping.

V. EFFECTS OF SYMMETRY IN 3-BAND CASES

In this section we study the effect of the CS in 3-band cases by setting $V = \pi/3$ in $U'_{\text{DKL}}(k_y)$ and $b = 2\pi/3$ in $U'_{\text{KHL}}(k_y)$, respectively. With such a parameter choice, the unit cell consists of 3 sites in both models. A similar procedure as mentioned for the 2-band case may be performed here. We first take periodic boundary conditions along x and y . Then, introducing three sets of $|\bar{k}_x\rangle$ states which are Bloch-periodic over 3 sites, we may reduce the Floquet operators to the form

$$U(k_y) = \sum_{\bar{k}_x} e^{-iH_{\text{eff}}(\bar{k}_x, k_y)} \otimes |\bar{k}_x\rangle \langle \bar{k}_x|, \quad (45)$$

where $H_{\text{eff}}(\bar{k}_x, k_y)$ is now a 3×3 matrix. By numerically diagonalizing these $H_{\text{eff}}(\bar{k}_x, k_y)$ across the entire (\bar{k}_x, k_y) BZ, we obtain 3 quasi-energy bands for both models. Since we

are now dealing with a $H_{\text{eff}}(\bar{k}_x, k_y)$ matrix of dimension $N \times N$ where N is odd, we turn to another topological invariant, the Chern number.

Denoting the eigenstates of either model as $|\psi_n(\bar{k}_x, k_y)\rangle$, where $n = 1, 2, 3$ is the band index, the Chern number of the n th band is given by

$$C_n = \frac{i}{2\pi} \oint d\mathbf{k} \cdot \langle \psi_n(\bar{k}_x, k_y) | \nabla_{\mathbf{k}} | \psi_n(\bar{k}_x, k_y) \rangle, \quad (46)$$

where $\mathbf{k} \equiv (\bar{k}_x, k_y)$. We have evaluated the Chern numbers of the bulk bands of both models for a wide range of parameters. To study the issue of bulk-edge correspondence, we diagonalize the two models numerically under open boundary conditions along x . We present in Figs. 4 and 5 the 3-band quasi-energy spectra for the DKL and KHL models respectively, over a wide range of parameters. Using our previous proof in Ref. [39], we choose the system parameters such that the respective panels of the two figures feature topologically equivalent bulk bands (i.e., always having precisely the same Chern numbers for all three bands).

One relatively well-known expectation regarding the bulk-edge correspondence here is as follows [11]: The Chern number of band n gives the net number of chiral modes with positive gradient localized on the left boundary with quasi-energy in the gap above the band subtracted by the net number of chiral modes with positive gradient localized on the left boundary with quasi-energy in the gap below it. A similar counting holds for the right edge, with the exception that we count the net number of chiral modes with negative gradient instead. We see that the above statement indeed holds true for both models in Figs. 4 and 5. However, we see that at large field strengths R for the KHL model, we see counter-propagating chiral modes within the same quasi-energy gap on the same edge with opposite group velocities [15], an oddity not seen in previously studied topological driven systems. These anomalous counter-propagating chiral edge modes were first pointed out in the work of [15]. In particular, Figs. 5(b) and 5(c) show these counter-propagating modes in the gap centered around the quasi-energy BZ borders at $\pm\pi$, while Fig. 5(d) shows the counter-propagating modes are present in both the quasi-energy gaps. Fig. 5(a) and 5(d) show strikingly that the Chern numbers are insufficient for determining the edge state behaviour of a Floquet system, since both panels show the same Chern numbers while exhibiting totally different edge modes.

The question is then, can we use again the previously constructed CS operators to explain

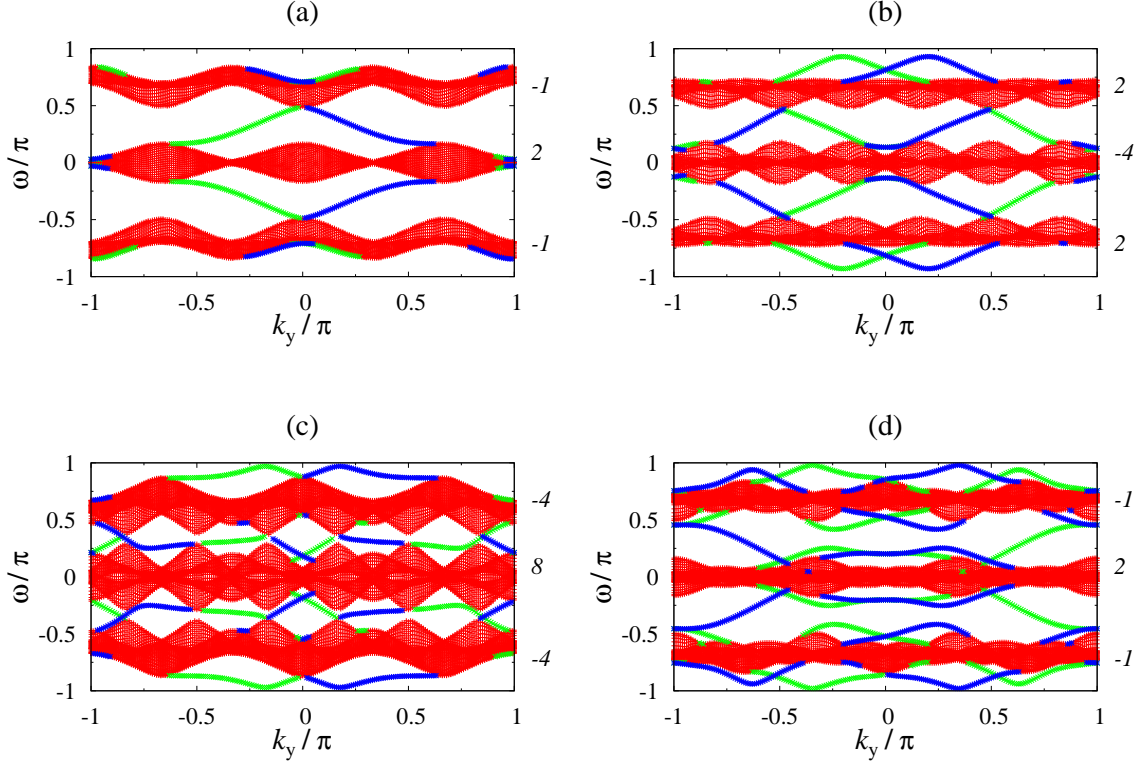


FIG. 4. (color online). The QE spectra for the double kicked lattice model at $V = \pi/3$, $J_2 = 2\pi/3$ and (a) $J_1 = \pi$, (b) $J_2 = 2\pi$, (c) $J_2 = 2.4\pi$, (d) $J_2 = 3\pi$. The chiral edge modes on the left (right) edges of the system are indicated in green (blue). The Chern numbers of the bands are indicated on the right of each spectrum.

the existence of the counter-propagating edge states at $\omega = \pm\pi$ in the KHL model and the absence of such states in the DKL model? The rest of this section is devoted to this question and our answer is again yes.

Under open boundary conditions along x , the DKL model Floquet operator obeys

$$\Gamma_{\text{DK}} U'_{\text{DKL}}(k_y) \Gamma_{\text{DK}} = U'^{\dagger}_{\text{DKL}}(k_y), \quad (47)$$

where as the KHL model Floquet operator obeys

$$\Gamma_{\text{KH}} U'_{\text{KHL}}(k_y) \Gamma_{\text{KH}} = U'^{\dagger}_{\text{KHL}}(k_y + \pi). \quad (48)$$

This means that, as already mentioned previously, that given the existence of a state with quasi-energy ω at k_y , the CS of the KHL implies the existence of a state with quasi-energy

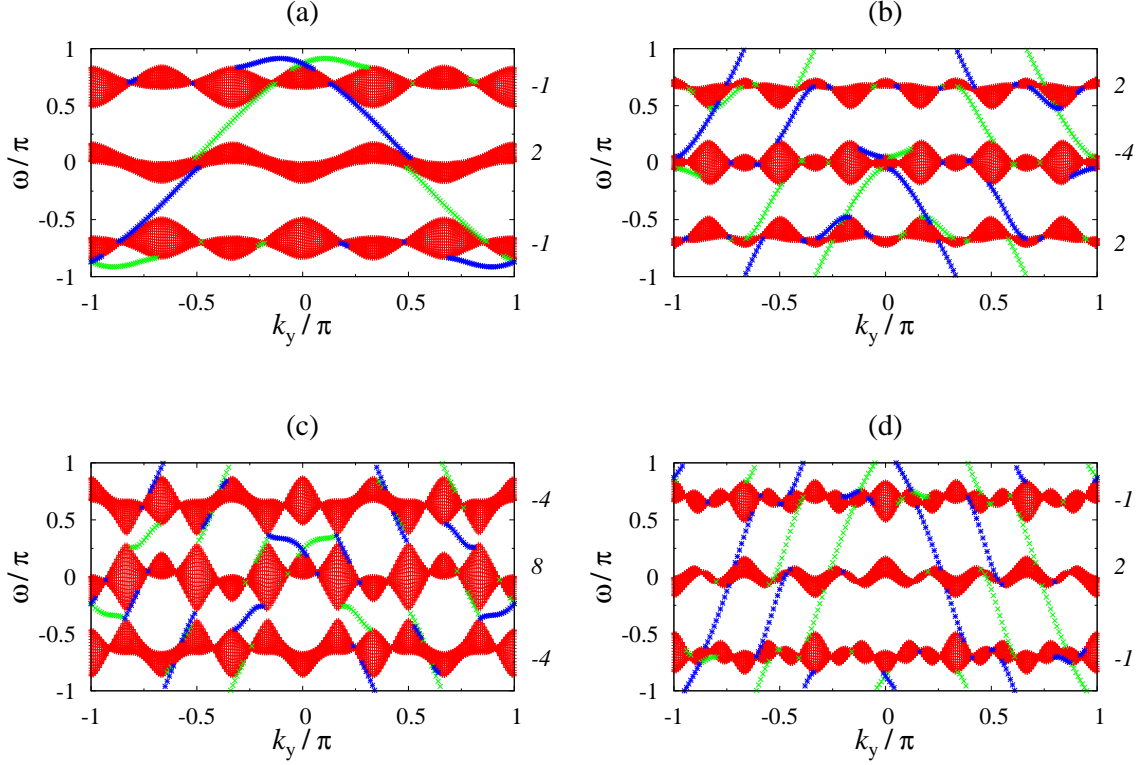


FIG. 5. (color online). The QE spectra for the kicked Harper lattice model at $b = 2\pi/3$, $J = 2\pi/3$ and (a) $R = \pi$, (b) $R = 2\pi$, (c) $R = 2.4\pi$, (d) $R = 3\pi$. The chiral edge modes on the left (right) edges of the system are indicated in green (blue). The Chern numbers of the bands are indicated on the right of each spectrum.

$-\omega$ at $k_y + \pi$. As already pointed out in Ref. [15], with which our results concur totally, the above result applied to chiral edge modes crossing the quasi-energy Brillouin zone (BZ) border at $\omega \pm \pi$ means the following: for any chiral edge mode crossing say upwards through $\omega = \pi$ at arbitrary k_y on a particular edge, there must be another chiral edge mode crossing downwards through $\omega = -\pi$ at $k_y + \pi$ on the *same* edge. These two edge modes must be on the same edge because Γ_{KH} is a local operator (i.e., it does not translate wavefunctions across the lattice space). These two chiral edge modes then form an anomalous pair of counter-propagating edge modes. Similar arguments apply for chiral modes crossing the quasi-energy BZ downwards through $\omega = -\pi$ at arbitrary k_y . These statements may be easily verified by visual inspection of Fig. 5. This hence explains why the KHL can support these novel counter-propagating edge modes living on the same edge and in the same gap.

Remarkably, the situation is totally different for the DKL model. Eq. (47) reveals that the presence of CS implies that given the existence of an eigenstate with quasi-energy ω at some k_y , there must always be an eigenstate of quasi-energy $-\omega$ at the *same* k_y . Hence, in the DKL model, if we have an edge mode with quasi-energy $\omega = \pi$ at k_y , there will also be an edge mode with quasi-energy $\omega = -\pi$ at the same k_y localized on the same edge. The fact that these two states exist on the same edge and have equal quasi-energies with the *same* k_y means that the states will mix and in general an avoided crossing will occur at $\omega = \pm\pi$ at that particular k_y value. The above statements are clearly consistent with the edge spectra seen in Fig. 4. Since the edge states cannot traverse the gap at $\pm\pi$, they are by definition not chiral edge modes. Nonetheless, we still do have counter-propagating edge modes on the same edge in the same gap. This can be seen in Figs. 4(b)-(d) in the topmost and bottommost gaps. These edge modes which creep out from the top and bottom bands only to be turned back at avoided crossings have not, to the best of our knowledge, been carefully studied in the literature and thus may constitute a new object in the currently still-developing understanding of bulk-edge correspondence in periodically driven systems.

VI. EXPERIMENTAL REALIZATION

We discuss first the 2-band case of the DKL Floquet operator. One possible method of observing the topological zero modes is to adapt the waveguide array used in the experiments of [48] (see also [49]). In this setup, a 1D array of evanescently coupled waveguides simulates a quantum particle in a tight-binding lattice, with the propagation distance down the arrays playing the role of time. In these experiments, light injected into a single waveguide simulates a quantum particle with initial state localized at one single lattice site. As the light travels down the waveguide, it spreads into neighbouring waveguides due to the evanescent coupling. This simulates the hopping of the particle between adjacent tight binding lattice sites as a function of time. The intensity profile (i.e., intensity plotted against the positions of waveguides) of the light beam at different propagation distances as a function of the waveguides then gives us the probability density of the simulated particle's wavefunction as a function of time. Different on-site potential terms in a tight-binding lattice are simulated by tuning the refractive indices of individual waveguides. Different nearest-neighbour hopping terms are simulated by varying the distances between neighbouring waveguides. The

output intensity profile, corresponding to the wavefunction density profile at a certain time, is obtained by terminating the waveguides at the corresponding propagation distance and recording the light intensities exiting the waveguides using an infra-red camera.

Using this setup, the four stages of Eq. (2) for a single 1D descendant $U_{\text{DKL}}(k_y)$ should be realizable. This means that we are simulating a 1D tight-binding lattice under open boundary conditions. We index the waveguides/lattice sites as n_x and choose a single arbitrary value of k_y for which 0 and/or π modes are present. To realize the 2-band $U_{\text{DKL}}(k_y)$ Floquet operator, a different tight-binding Hamiltonian (tbh) must be simulated during each stage. The first stage consists of realizing a nearest neighbour tbh of the form

$$\sum_{n_x} (e^{ik_y} |n_x + 1\rangle \langle n_x| + \text{h.c.}) .$$

In the experiments of [48], the hopping amplitudes realized are all purely real numbers, meaning that complex hopping amplitudes like e^{ik_y} above are not directly realizable. However, we may rewrite the $U_{\text{DKL}}(k_y)$ operator as

$$U_{\text{DKL}}(k_y) = e^{i\hat{n}_x^2\pi} e^{-iJ_2 \cos(\hat{k}_x)} e^{-i\hat{n}_x^2\pi} e^{i\hat{n}_x k_y} e^{-iJ_1 \cos(\hat{k}_x)} e^{i\hat{n}_x k_y} . \quad (49)$$

Hence, the first stage of evolution now consists of three sub-stages, during each of which a different tbh is needed. The first stage is simply an on-site evolution of the form

$$\sum_{n_x} (-\hat{n}_x k_y + l_{n_x} \times 2\pi) |n_x\rangle \langle n_x| ,$$

where the integers l_{n_x} are chosen so that each on-site term is of a reasonable value. We note that this freedom results from the fact that the tbh required to realize $e^{i\hat{n}_x k_y}$ is not uniquely defined since phases are only defined modulo 2π . This tbh may be realized using the waveguide array setup by engineering the separation between nearest neighbour waveguides to be very large, so that hopping is negligible. The on-site terms $n_x k_y$ can then be realized by setting the refractive index of each waveguide accordingly as was done in [48]. The next sub-stage is a nearest-neighbour hopping term which is realized by bringing the waveguides closer together again to allow hopping of light between waveguides and also changing the refractive indices of all waveguides to be equal, so that the on-site term is then simply a physically meaningless additive constant in the tbh which may be ignored. The third sub-stage is then realized in a manner entirely similar to the first sub-stage.

Moving on to the second stage of $U_{\text{DKL}}(k_y)$ which is the operator $e^{-i\hat{n}_x^2\pi}$, we note that this corresponds simply to tagging a phase factor of $e^{-i\pi/2} = -i$ for odd sites and a phase factor of unity for even sites. The operator $e^{-i\hat{n}_x^2\pi}$ may thus just as well be replaced by $\exp[-i\sin^2(\hat{n}_x^2\frac{\pi}{2})]$. This operator may be realized in the waveguide array by again keeping the waveguides far apart so that tunnelling is negligible and tuning the refractive indices accordingly. The third stage of $U_{\text{DKL}}(k_y)$ is again just a nearest neighbour hopping equivalent to the second sub-stage of the first stage discussed earlier. The fourth stage is very similar to the second stage. The operator $e^{i\hat{n}_x^2\pi}$ may be replaced by the operator $\exp[i\sin^2(\hat{n}_x^2\frac{\pi}{2})]$. It is also similarly realized by keeping the waveguide spacing large in order to suppress tunnelling while tuning the refractive indices accordingly. There are two potential major difficulties in carrying out the above experiment. The first would be changing the refractive index of the waveguides as a function of propagation distance, something which was not done in [48]. The second difficulty would be suppressing the tunnelling to effectively zero in the second and fourth stages, as this requires making the waveguides suddenly move far apart from each other as a function of propagation distance.

The above waveguide array simulates one iteration of the Floquet operator $U_{\text{DKL}}(k_y)$ on a particle in a tight-binding lattice. To confirm the existence of edge modes, we need only inject light into the waveguide at the edge of the array where the edge modes are predicted to exist and record the intensity profile at the other end of the array. We should find that in the cases where edge modes are predicted, the light will remain confined along the edge of the array as it propagates down the waveguides. The π modes may be distinguished from the 0 modes by repeating the above waveguide protocol several times, thus simulating several periods of the double kicked lattice Hamiltonian. The π modes will then manifest as repetitions of the output intensity profile over every two “periods” (ie. after the light has passed through two simulated iterations of $U_{\text{DKL}}(k_y)$, some part of the initial beam will reappear at its initial position). We note that similar protocols may be followed using the waveguide array setup to realize the 2-band $U_{\text{KHL}}(k_y)$ operator. In this case, we should find that injecting a beam into a waveguide at the edge should always result in the beam spreading into the bulk of the waveguides since no edge modes exist.

We move on to discuss the 3-band cases. Our interest here is mainly to study the 3-band 2D KHL Floquet operator U_{KHL} in order to observe the propagation of the chiral edge modes. Possible experimental realization of the U_{KHL} has been discussed in the work of [15]. The

authors suggest realizing the model by making use of artificial magnetic field techniques [50] or by introducing complex tunnelling amplitudes via shaking an optical lattice [51]. They suggest that the anomalous counter-propagating modes may be identified using the momentum-resolved photoemission spectroscopy method of [52] which extracts a spectral function which yields information on the number of states present for each energy and each momentum.

We focus our attention next on the realization of the 3-band 2D DKL Floquet operator U_{DKL} . The 3-band Floquet operator is given by

$$U_{\text{DKL}} = e^{-i\hat{n}_x^2 \frac{\pi}{3}} e^{-iJ_1 \cos(\hat{k}_x + \hat{k}_y)} e^{i\hat{n}_x^2 \frac{\pi}{3}} e^{-iJ_2 \cos(\hat{k}_x)}, \quad (50)$$

where we have re-ordered the four stages of evolution for easier explanation. This operator may be realized in a 2D cold atom setup. We begin with spinless fermionic atoms in a deep 2D square lattice. The atoms are prepared in the ground state which consists of a filled lowest Bloch band with all upper bands unoccupied. The first stage of evolution, described by the operator $e^{-iJ_2 \cos(\hat{k}_x)}$, may be realized by lowering the potential barriers between adjacent sites along the x direction, while keeping the barriers between sites along y high so that to a good approximation tunnelling y is totally suppressed. To realize the next stage, which is described by $e^{i\hat{n}_x^2 \frac{\pi}{3}}$, we ramp up the lattice heights along both x and y directions to suppress all tunnelling and switch on an inverted superlattice harmonic potential $-x^2 \times \pi/3$, with no y -dependence for one unit of time. The third stage, described by $e^{-iJ_1 \cos(\hat{k}_x + \hat{k}_y)}$ is somewhat tricky. Here we need to switch off the first 2D optical lattice mentioned in the first stage, and switch on a second 2D lattice which only allows hopping in a diagonal direction along the original square lattice and forbids all other hoppings. This is equivalent to realizing a checkerboard lattice in an $x-y$ coordinate system which is rotated by angle of 45° about the z -axis relative to the original coordinate system in which the optical lattice takes the form of a square lattice. The fourth and final stage described by $e^{i\hat{n}_x^2 \frac{\pi}{3}}$ is realized by reverting back to the square and switching on a harmonic potential $-x^2 \times \pi/3$. The edge states can then be observed using the direct imaging method of [53] or the photoemission method of [52].

VII. CONCLUDING REMARKS

Irrespective of the details presented in this work, the first important message from this paper is that even one-dimensional, deceptively simple, driven quantum systems can already generate many different topological states of matter. This strongly hints the usefulness of a control field in the active creation of desirable topological states of matter. Since the models used in this work are originally from the quantum chaos literature, it is interesting to see how current experimental research activities on quantum dynamical systems (as well as some existing theoretical tools in the literature, see, for example, Ref. [30, 54]) may soon become useful in exploring novel topological states.

As for specific results, we have analysed dynamical models possessing chiral symmetry. In spite of the explicit mapping between these two models (and hence precisely the same Chern numbers when they are computable), their edge modes are totally different. The differences are found to be due to the particular form of the chiral symmetry operator associated with the Floquet operators. This indicates that in general, in order to predict the edge state behaviour of a periodically driven system, it is important not only to find its obeyed symmetries but also to take into account the nature of the symmetry operator concerned (in our case, the chiral symmetry operator). These results also suggest that a full topological classification of periodically driven systems cannot be obtained by straightforwardly transplanting the static tenfold classification [20]. Specific symmetry properties will be important when developing a full picture of bulk-edge correspondence in driven systems.

Throughout this work, we have focused on 2-band or 3-band cases. On the computational side, it is straightforward to extend our consideration to cases with more bands. We note that we indeed carried out many calculations for cases with many Floquet bands. The observations made in this work regarding the difference between DKL and KHL still hold. That is, if the number of bands is even, then there exist many edge models with 0 or π quasi-energy values in the former model (DKL) but not in the latter (KHL); and if the number of bands is odd, there exist many counter-propagating chiral edge modes in the latter but not in the former. These additional results indicate that our observed effects of symmetry on edge states are general. In future, it would be also interesting to study the implications of particular properties of other symmetry operators, such as time-reversal or particle-hole symmetry operators, for the issue of bulk-edge correspondence.

For possible experimental interests, before ending we highlight that a simple driven lattice model (the DKL) is able to host an arbitrarily large number of topologically protected 0 and π quasi-energy edge modes. These modes could be useful for future quantum information applications [55]. We note also that photonic setups are increasingly establishing themselves as a versatile setup for simulating topological quantum phases [9, 56]. It will be interesting to explore in more detail how such setups may be used to further explore topological phases.

Appendix A: On the properties of CS operators of DKL and KHL

In this Appendix A, we present some details regarding the difference in the chiral symmetry operators. We begin by noting that

$$\begin{aligned}\Gamma_{\text{DK}} U'_{\text{DKL}} \Gamma_{\text{DK}}^\dagger &= \sum_{k_y} e^{i\hat{n}_x \pi} U'_{\text{DKL}}(k_y) e^{-i\hat{n}_x \pi} \otimes |k_y\rangle \langle k_y| \\ &= \sum_{k_y} U'_{\text{DKL}}(k_y)^{-1} \otimes |k_y\rangle \langle k_y|,\end{aligned}\tag{A1}$$

where in the first line we made use of the fact that the CS operator Γ_{DK} has no dependence on \hat{n}_y or \hat{k}_y and thus has no effect on the $|k_y\rangle$ states (ie. we can simply move the $\Gamma_{\text{DK}}^\dagger$ past the projectors $|k_y\rangle \langle k_y|$). The above equation shows that so long as the 2D ancestor U'_{DKL} obeys the CS condition of Eq. (8) with the CS operator $\exp(i\hat{n}_x \pi)$, so too will all of its 1D descendents $U'_{\text{DKL}}(k_y)$.

The situation is quite different for the KHL because its CS operator $\Gamma_{\text{KH}} = e^{(i\hat{n}_x \pi)} e^{(i\hat{n}_y \pi)}$ depends on \hat{n}_y . As such,

$$\Gamma_{\text{KH}} U'_{\text{KHL}} \Gamma_{\text{KH}}^\dagger = \sum_{k_y} e^{i\hat{n}_x \pi} U'_{\text{KHL}}(k_y) e^{-i\hat{n}_x \pi} \otimes |k_y - \pi\rangle \langle k_y - \pi|.\tag{A2}$$

One easily verifies using Eq. (16) that

$$\begin{aligned}e^{i\hat{n}_x \pi} U'_{\text{KHL}}(k_y) e^{-i\hat{n}_x \pi} &= U'_{\text{KHL}}(k_y - \pi)^{-1} \\ &\neq U'_{\text{KHL}}(k_y)^{-1}.\end{aligned}\tag{A3}$$

This means that while the ancestor 2D operator U'_{KHL} possesses CS, this does not pass on to the individual 1D descendents $U'_{\text{KHL}}(k_y)$.

It is now possible to better understand the topological protection of the edge modes with 0 and π quasi-energy values in the DKL model. We first set up some notation. On the 0

and π quasi-energy subspaces, Γ_{DK} and $U'_{\text{DKL}}(k_y)$ commute. This is easily seen as follows. Firstly, $U'_{\text{DKL}}(k_y)\Gamma_{\text{DK}} = \Gamma_{\text{DK}}U'^{\dagger}_{\text{DKL}}(k_y)$ due to the CS condition. Since any 0 or π quasi-energy eigenstate of $U'_{\text{DKL}}(k_y)$ is also an eigenstate of $U'^{\dagger}_{\text{DKL}}(k_y)$ with the same eigenvalue, Γ_{DK} and $U'_{\text{DKL}}(k_y)$ thus commute within the $\omega = 0$ and π subspaces. The commutation enables us to choose the 0 and π quasi-energy states to be common eigenstates of Γ_{DK} and $U'_{\text{DKL}}(k_y)$. Note that because $(\Gamma_{\text{DK}})^2 = \mathbb{1}_x$, its only possible eigenvalues are ± 1 . This allows us to define two sublattices [10] denoted A and B , with projectors $\Pi_A = (1 + \Gamma_{\text{DK}})/2$ and $\Pi_B = (1 - \Gamma_{\text{DK}})/2$ respectively (ie. sublattice A (B) consists of all the even (odd) sites). Each 0 or π quasi-energy state then resides entirely on one lattice only. We denote such eigenstates as $|\psi_{\omega,j}^{(\alpha)}\rangle$, where $\omega = 0, \pi$, $\alpha \equiv A, B$ and j is an index to label different states in the event that we have multiple eigenstates with the same quasi-energy and same sublattice index α .

Now, assume that at some k_y , we happen to have a number of 0 and π quasi-energy states. Suppose we perturb the system in a way which preserves the chiral symmetry of Eq. (17). We may regard this increase as adding a CS-preserving perturbation to the original $\hat{H}'_{\text{eff}}(k_y)$, defined by $U'_{\text{DKL}}(k_y) \equiv e^{-i\hat{H}'_{\text{eff}}(k_y)}$. We denote this perturbation as \hat{H}_p . By definition of preservation of CS, it must be true that the anti-commutator $\{\Gamma_{\text{DK}}, \hat{H}_p\}$ vanishes. We consider the following matrix element of this anti-commutator,

$$\langle \psi_{\omega,j}^{(\alpha)} | \{\Gamma_{\text{DK}}, \hat{H}_p\} | \psi_{\omega',j'}^{(\alpha')} \rangle = 0. \quad (\text{A4})$$

This tells us that a CS-preserving perturbation cannot mix two states living on the same sublattice. That is, \hat{H}_p can only mix edge states living on different sublattices. If we interpret the tuning of k_y in $U'_{\text{DKL}}(k_y)$ as a CS-preserving perturbation, then it is expected that the number of protected 0 and π -quasi-energy edge states remains constant as we tune k_y so long as no touching between the two bulk bands occurs. And if the bands touch at quasi-energy 0 or π , then the edge modes will become delocalized into the bulk.

The above analysis does not apply to the KHL model because the starting point of the analysis, which is the presence of CS in the 1D descendent Floquet operator, is not true for the KHL. This finally explains the big difference in edge states between DKL and KHL.

Appendix B: Explicit Forms of $U''_{\text{DKL}}(k_y)$ in the 2-band case

The Floquet operator $U''_{\text{DKL}}(k_y)$ in \bar{k}_x representation and its effective Hamiltonian are written out below.

$$U''_{\text{DKL}}(k_y) \equiv \sum_{\bar{k}_x} e^{-i \sum_{\bar{k}_x} H''_{\text{eff}}(\bar{k}_x, k_y) \otimes |\bar{k}_x\rangle \langle \bar{k}_x|}, \quad (\text{B1})$$

where

$$\begin{aligned} H''_{\text{eff}}(\bar{k}_x, k_y) &= \mathbf{h}''(\bar{k}_x, k_y) \cdot \sigma, \\ \mathbf{h}''(\bar{k}_x, k_y) &= E(\bar{k}_x, k_y) \mathbf{n}''(\bar{k}_x, k_y), \\ \mathbf{n}''(\bar{k}_x, k_y) &= [n''_x(\bar{k}_x, k_y), n''_y(\bar{k}_x, k_y), 0], \\ n''_x(\bar{k}_x, k_y) &= \frac{\cos(\frac{\bar{k}_x}{2}) \cos(P) \sin(Q) + \sin(\frac{\bar{k}_x}{2}) \sin(P)}{\sin[E(\bar{k}_x, k_y)]}, \\ n''_y(\bar{k}_x, k_y) &= \frac{-\sin(\frac{\bar{k}_x}{2}) \cos(P) \sin(Q) + \cos(\frac{\bar{k}_x}{2}) \sin(P)}{\sin[E(\bar{k}_x, k_y)]}, \end{aligned} \quad (\text{B2})$$

and $E(\bar{k}_x, k_y), P, Q$ are as they were defined previously.

Appendix C: on the edge states at different sublattices of the 2-band DKL model

Following Ref. [10], here we discuss a connection between the edge states of the two symmetric time frames. We start off by considering the edge eigenstates of say the single-primed Floquet operator $U'_{\text{DKL}}(k_y)$. We choose these to be common eigenstates of $U'_{\text{DKL}}(k_y)$ and Γ_{DK} so that each state is supported completely on only one sublattice. We denote these states as $|\psi_{\omega, c}\rangle$ with quasi-energy $\omega = 0$ or π , with c representing the eigenvalue with respect to Γ_{DK} , so that $c = 1$ (-1) if it lies on the A (B) sublattice. These states obey $\hat{F}\hat{G}|\psi_{\omega, c}\rangle = e^{-i\omega}|\psi_{\omega, c}\rangle$. Next, we define states

$$|\Phi_{\omega, c'}\rangle \equiv \hat{G}|\psi_{\omega, c}\rangle. \quad (\text{C1})$$

It is easy to see that these states are eigenstates of $U''_{\text{DKL}}(k_y)$ with the same quasi-energy ω (simply act $\hat{G}\hat{F}$ on both sides of Eq. (C1) and simplify.). We now show that these states are also eigenstates of Γ_{DK} with eigenvalue $c' = e^{i\omega}c$. Beginning from Eq. (C1), we act \hat{F} on both sides of the equation and rearrange to obtain

$$\hat{F}^{-1}|\psi_{\omega, c}\rangle = e^{i\omega}|\Phi_{\omega, c'}\rangle. \quad (\text{C2})$$

This will be useful shortly. Next, we act Γ_{DK} on both sides of Eq. (C1) and make use of $\Gamma_{\text{DK}}\hat{G}\Gamma_{\text{DK}} = \hat{F}^{-1}$ to obtain

$$\Gamma_{\text{DK}}|\Phi_{\omega,c'}\rangle = \hat{F}^{-1}c|\psi_{\omega,c}\rangle.$$

We now substitute Eq. (C2) into the above equation's right hand side and obtain our desired result that

$$\Gamma_{\text{DK}}|\Phi_{\omega,c'}\rangle = e^{i\omega}c|\Phi_{\omega,c}\rangle, \quad (\text{C3})$$

meaning that $|\Phi_{\omega,c'}\rangle$ is an eigenstate of Γ_{DK} with eigenvalue $c' = e^{i\omega}c$. Applying this observation to $\omega = 0$ or $\omega = \pi$, one sees that the $\omega = 0$ edge states in the two symmetric frames live on the same sublattice, while the $\omega = \pi$ edge states in the two symmetric frames live on different sublattices.

-
- [1] T. Kitagawa, M. S. Rudner, E. Berg, and E. Demler, Phys. Rev. A **82**, 033429 (2010).
 - [2] T. Kitagawa, E. Berg, M. Rudner, and E. Demler, Phys. Rev. B **82**, 235114 (2010).
 - [3] L. Jiang, T. Kitagawa, J. Alicea, A. R. Akhmerov, D. Pekker, G. Refael, J. I. Cirac, E. Demler, M. D. Lukin, and P. Zoller, Phys. Rev. Lett. **106**, 220402 (2011).
 - [4] N. H. Lindner, G. Refael, and V. Galitski, Nat. Phys. **7**, 490 (2011).
 - [5] D. Y. H. Ho and J. B. Gong, Phys. Rev. Lett. **109**, 010601 (2012).
 - [6] J. K. Asbóth, Phys. Rev. B **86**, 195414 (2012).
 - [7] T. Kitagawa, M. A. Broome, A. Fedrizzi, M. S. Ruder, E. Berg, I. Kassal, A. Aspuru-Guzik, E. Demler, and A. G. White, Nat. Commun. **3**, 882 (2012).
 - [8] B. Dóra, J. Cayssol, F. Simon, and R. Moessner, Phys. Rev. Lett. **108**, 056602 (2012).
 - [9] M. C. Rechtsman, J. M. Zeuner, Y. Plotnik, Y. Lumer, D. Podolsky, F. Dreisow, S. Nolte, M. Segev, and A. Szameit, Nature **496**, 196 (2013).
 - [10] J. K. Asbóth and H. Obuse, Phys. Rev. B **88**, 121406 (2013).
 - [11] M. S. Rudner, N. H. Lindner, E. Berg, and M. Levin, Phys. Rev. X **3**, 031005 (2013).
 - [12] M. Thakurathi, A. Patel, D. Sen, and A. Dutta, Phys. Rev. B **88**, 155133 (2013).
 - [13] Y. T. Katan, and D. Podolsky, Phys. Rev. Lett. **110**, 016802 (2013).
 - [14] Q. Tong, J. An, J. B. Gong, H. Luo, and C. H. Oh, Phys. Rev. B **87**, 201109 (2013).
 - [15] M. Lababidi, I. I. Satija, and E. Zhao, Phys. Rev. Lett. **112**, 026805 (2014).

- [16] G. Puentes, I. Gerhardt, F. Katzschnann, C. Silberhorn, J. Wrachtrup, and M. Lewenstein
Phys. Rev. Lett. **112**, 120502 (2014).
- [17] Y. Hatsugai, Phys. Rev. B **48**, 11851 (1993).
- [18] Y. Hatsugai, Phys. Rev. Lett. **71**, 3697 (1993).
- [19] M. Z. Hasan and C. L. Kane, Rev. Mod. Phys. **82**, 3045 (2010).
- [20] R. Shinsei, A. P. Schnyder, A. Furusaki, and A. W. W. Ludwig, New J. Phys. **12**, 065010
(2010); M. R. Zirnbauer, J. Math. Phys. **37**, 4986 (1996); A. Altland and M. R. Zirnbauer,
Phys. Rev. B **55**, 1142 (1997).
- [21] G.M. Zaslavskii, M.Yu. Zakharov, R. Z. Sagdeev, D.A.Usikov, and A. A. Chernikov, Sov.
Phys. JETP **64**, 294 (1986).
- [22] R. Lima and D. Shepelyansky, Phys. Rev. Lett. **67**, 1377 (1991).
- [23] T. Geisel, R. Ketzmerick, and G. Petschel, Phys. Rev. Lett. **67**, 3635 (1991).
- [24] P. Leboeuf, J. Kurchan, M. Feingold, and D. P. Arovas, Phys. Rev. Lett. **65**, 3076 (1990); P.
Leboeuf, J. Kurchan, M. Feingold, and D. P. Arovas, Chaos, **2**, 125 (1992).
- [25] R. Artuso, F. Borgonovi, I. Guarneri, L. Rebuzzini, and G. Casati, Phys. Rev. Lett. **69**, 3302
(1992).
- [26] R. Artuso, G. Casati, and D. Shepelyansky, Phys. Rev. Lett. **68**, 3826 (1992).
- [27] R. Ketzmerick, G. Petschel, and T. Geisel, Phys. Rev. Lett. **69**, 695 (1992).
- [28] R. Roncaglia, L. Bonci, F. M. Izrailev, B. J. West, and P. Grigolini, Phys. Rev. Lett. **73**, 802
(1994).
- [29] I. Dana, Phys. Lett. A **197**, 413 (1995).
- [30] I. Dana, Phys. Rev. E **52**, 466 (1995).
- [31] R. Ketzmerick, K. Kruse, and T. Geisel, Phys. Rev. Lett. **80**, 137 (1998).
- [32] T. Prosen, I. I. Satija, and N. Shah, Phys. Rev. Lett. **87**, 066601 (2001).
- [33] P. H. Jones, M. M. Stocklin, G. Hur, and T. S. Monteiro, Phys. Rev. Lett. **93**, 223002 (2004).
- [34] J. Wang and J. B. Gong, Phys. Rev. A **77**, 031405 (2008).
- [35] J. Wang, A. S. Mouritzen, and J. B. Gong, J. Mod. Opt. **56**, 722 (2009).
- [36] W. Lawton, A. S. Mouritzen, J. Wang, and J. B. Gong, J. Math. Phys. **50**, 032103 (2009).
- [37] J. Wang, I. Guarneri, G. Casati, and J. B. Gong, Phys. Rev. Lett. **107**, 234104 (2011); H.
Wang, J. Wang, I. Guarneri, G. Casati, and J. B. Gong, Phys. Rev. E **88**, 052919 (2013).
- [38] J. Wang and J. B. Gong, Phys. Rev. E **78**, 036219 (2008).

- [39] H. Wang, D. Y. H. Ho, W. Lawton, J. Wang, and J. B. Gong, Phys. Rev. E **88**, 052920 (2013).
- [40] The explicit mapping is given by Eq. (21) in Ref. [39] in cases with an odd of Floquet bands. For cases with an even number of Floquet bands, a slightly different mapping can be constructed as well (H. L. Wang and J. B. Gong, unpublished).
- [41] D. R. Hofstadter, Phys. Rev. B **14**, 2239 (1976).
- [42] I. Dana, E. Eisenberg, and N. Shnerb, Phys. Rev. E **54**, 5948 (1996).
- [43] J. B. Gong and J. Wang, Phys. Rev. E **76**, 036217 (2007).
- [44] T. Boness, S. Bose, and T. S. Monteiro, Phys. Rev. Lett. **96**, 187201 (2006).
- [45] To be precise, the quasi-energy is defined as ω when the unitary eigenvalue of the Floquet operator is written as $e^{-i\frac{\omega T}{\hbar}}$, with T being the time period. Since we always have the freedom to set T and \hbar to one, for brevity we will just write the unitary eigenvalue of the Floquet operator as $e^{-i\omega}$ and refer to ω as the quasi-energy.
- [46] The lattice sites $|n_{x(y)}\rangle$ here are mathematically equivalent to the discrete angular momentum eigenstates considered in the original ORDKR and KHM where a particle on a ring (i.e., a rotator space) was considered.
- [47] D. Sticlet and F. Piéchon, Phys. Rev. B **87**, 115402 (2013).
- [48] Y. E. Kraus, Y. Lahini, Z. Ringel, M. Verbin, and O. Zilberberg, Phys. Rev. Lett. **109**, 106402 (2012).
- [49] S. Ganeshan, K. Sun, and S. D. Sarma, Phys. Rev. Lett. **110**, 180403 (2013).
- [50] Y. J. Lin, R. L. Compton, K. Jimenez-Garcia, J. V. Porto, and I. B. Spielman, Nature (London) **462**, 628 (2009); M. Aidelsburger, M. Atala, S. Nascimbène, S. Trotzky, Y.-A. Chen, and I. Bloch, Phys. Rev. Lett. **107**, 255301 (2011).
- [51] J. Struck, C. Ölschläger, M. Weinberg, P. Hauke, J. Simonet, A. Eckardt, M. Lewenstein, K. Sengstock, and P. Windpassinger, Phys. Rev. Lett. **108**, 225304 (2012); P. Hauke, O. Tieleman, A. Celi, C. Ölschläger, J. Simonet, J. Struck, M. Weinberg, P. Windpassinger, K. Sengstock, M. Lewenstein, and A. Eckardt, Phys. Rev. Lett. **109**, 145301 (2012).
- [52] J. T. Stewart, J. P. Gaebler, and D. S. Jin, Nature (London) **454**, 744 (2008).
- [53] N. Goldman, J. Dalibard, A. Dauphin, F. Gerbier, M. Lewenstein, P. Zoller, and I. B. Spielman, Proc. Natl. Acad. Sci. U.S.A. **110**, 6736 (2013).
- [54] I. Dana, M. Feingold, and M. Wilkinson, Phys. Rev. Lett. **81**, 3124 (1998).
- [55] D. E. Liu, A. Levchenko, and H. U. Baranger, Phys. Rev. Lett. **111**, 047002 (2013).

[56] M. Pasek and Y. D. Chong, Phys. Rev. B **89**, 075113 (2014).